Video Article

Integrating a Triplet-triplet Annihilation Up-conversion System to Enhance Dye-sensitized Solar Cell Response to Sub-bandgap Light

Andrew Nattestad[1], Yuen Yap Cheng[2], Rowan W. MacQueen[2], Gordon G. Wallace[1], Timothy W. Schmidt[3]

[1]ARC Centre of Excellence for Electromaterials Science (ACES), Intelligent Polymer Research Institute (IPRI), The University of Wollongong

[2]School of Chemistry, The University of Sydney

[3]School of Chemistry, The University of New South Wales

Correspondence to: Timothy W. Schmidt at t.schmidt@unsw.edu.au

URL: https://www.jove.com/video/52028
DOI: doi:10.3791/52028

Keywords: Physics, Issue 91, Third generation photovoltaics, upconversion, organic electronics, device architecture, porphyrins, photovoltaic testing

Date Published: 9/12/2014

Citation: Nattestad, A., Cheng, Y.Y., MacQueen, R.W., Wallace, G.G., Schmidt, T.W. Integrating a Triplet-triplet Annihilation Up-conversion System to Enhance Dye-sensitized Solar Cell Response to Sub-bandgap Light. *J. Vis. Exp.* (91), e52028, doi:10.3791/52028 (2014).

Abstract

The poor response of dye-sensitized solar cells (DSCs) to red and infrared light is a significant impediment to the realization of higher photocurrents and hence higher efficiencies. Photon up-conversion by way of triplet-triplet annihilation (TTA-UC) is an attractive technique for using these otherwise wasted low energy photons to produce photocurrent, while not interfering with the photoanodic performance in a deleterious manner. Further to this, TTA-UC has a number of features, distinct from other reported photon up-conversion technologies, which renders it particularly suitable for coupling with DSC technology. In this work, a proven high performance TTA-UC system, comprising a palladium porphyrin sensitizer and rubrene emitter, is combined with a high performance DSC (utilizing the organic dye D149) in an integrated device. The device shows an enhanced response to sub-bandgap light over the absorption range of the TTA-UC sub-unit resulting in the highest figure of merit for up-conversion assisted DSC performance to date.

Video Link

The video component of this article can be found at https://www.jove.com/video/52028/

Introduction

Dye-sensitized solar cells (DSCs) have been proclaimed as a promising concept in affordable solar energy collection[1-3]. In spite of this enthusiasm, widespread commercialization has yet to occur. A number of reasons have been put forward for this, with one pressing issue being the relatively high energy of the absorption onset, limiting the achievable light harvesting efficiency of these devices[4]. Although this can be overcome, lowering the absorption onset is typically accompanied by a drop in open circuit voltage, which disproportionately erodes any gains in current density[5, 6].

The general operation of DSCs involves electron transfer from a photoexcited dye to a semiconductor (typically TiO_2), followed by the regeneration of the oxidized dye by a redox mediator. Both these processes appear to require substantial driving forces (potential) in order to proceed with high efficiency[7]. With such significant inherent losses, it becomes obvious that the optimal absorption onset for these devices is reasonably high in energy. Similar problems exist for organic photovoltaics (OPV), due once again to the large chemical driving forces required for effective charge separation. Accordingly, predictions of upper solar-to-electric conversion efficiency limits to single junction devices based on both of these technologies involve absorbers with wide (effective) band gaps[4].

In order to overcome the light harvesting issue raised above, a number of approaches have been taken. This includes the 'third generation'[8] approaches of tandem structures[9, 10] and photon upconversion[11-14].

Recently[11] we reported an integrated device composed of a DSC working and counter electrode, with a triplet-triplet annihilation based up-conversion (TTA-UC) system incorporated into the structure. This TTA-UC element was able to harvest red light transmitted through the active layer and chemically convert it (as described in detail below) to higher energy photons which could be absorbed by the active layer of the DSC and generate photocurrent. There are two important points to note about this system. Firstly, TTA-UC has many prospective advantages over other photon upconversion systems[11]; secondly it demonstrates a feasible architecture (proof-of-principle) for the incorporation of TTA-UC, which had been lacking from the TTA-UC literature up to that point.

The process of TTA-UC[15-24] involves the excitation of 'sensitizer' molecules, in this case Pd porphyrins, by light with energy below the device onset energy. The singlet-excited sensitizers undergo rapid intersystem crossing to the lowest-energy triplet state. From there, they can transfer energy to a ground-state triplet-accepting 'emitter' species such as rubrene, as long as the transfer is allowed by free energy[25]. The first triplet state of rubrene (T_1) is greater than half the energy of its first excited singlet state (S_1) but less than half the energy of T_2, meaning that an encounter complex of two triplet-excited rubrenes can annihilate to give one singlet excited emitter molecule (and the other in the ground state) with a fairly high probability. Other states, statistically predicted, are most likely energetically inaccessible for rubrene[26]. The singlet excited

rubrene molecule can then emit a photon (as per fluorescence) with energy sufficient to excite the dye on the working electrode of the DSC. This process is shown in **Animation 1**.

TTA-UC offers a number of advantages compared to other UC systems, such as a broad absorption range and incoherent nature[27, 28], making it an attractive option for coupling with DSC (as well as OPV). TTA-UC has been demonstrated operating at relatively low light intensities and in diffuse lighting conditions. Both DSC and OPV are most efficient in the low light intensity regime. Solar concentration is expensive and only justifiable for high efficiency, high cost devices. The relatively high performance of TTA-UC systems in low intensity lighting conditions is attributable to the process involving sensitizer chromophores with strong, broad absorption bands in concert with long-lived triplet states which are capable of diffusing in order to come into contact with interacting species. In addition, TTA-UC has been found to have high intrinsic efficiency from a kinetic study[26].

Although TTA-UC operates at low light intensity, there is still a quadratic relationship between incident light intensity and emitted light (at least at low light intensities). This is due to the bimolecular nature of the process. To account for this and the varied experimental conditions (particularly light intensity) reported by different groups, a figure of merit (FoM) system should be employed to meter the performance enhancement offered by upconversion. This FoM has been defined as $\Delta J_{SC}/\Theta$, where ΔJ_{SC} is the increase in short circuit current (usually determined by integration of the Incident Photon to Charge Carrier Efficiency, IPCE, with and without the upconversion effect) and Θ is the effective solar concentration (based on the photon flux in the relevant region, that is the Q-band absorption of the sensitizer)[229].

Herein, a protocol for producing and correctly characterizing an integrated DSC-TTA-UC device is reported, paying special attention to potential pitfalls in device testing. It is hoped that this will serve as a basis for further work in this field.

Protocol

1. DSC Fabrication

1.1. Working Electrode Preparation

1. Clean one whole sheet of F:SnO_2 coated glass (110 mm × 110 mm × 2.3 mm, <8 Ω/□) by sonication sequentially in soapy water, then acetone and finally ethanol (10 min each).
2. Deposit a dense layer of TiO_2 following the steps below:
    1. Dry glass using compressed air and heat glass to 450 °C on hotplate (conductive side up).
    2. Dilute Titanium diisopropoxide bis(acetylacetonate) (75 wt% in isopropanol) with ethanol in a 1:9 ratio.
    3. Spray the dilute solution onto heated glass from a distance of ~100 mm, with five sprays across the glass sheet.
    4. Spray one round per 10 sec for 12 rounds.
    5. Keep glass at 450 °C for a further 5 min, before switching off the hotplate. Leave the glass on hotplate and allow it to slowly cool to RT.
3. Place the glass onto the screen printer table (once again conductive side up). Insert screen and align pattern to glass. Add TiO_2 paste to screen and print one or two layers. If depositing two layers, remove glass plate from printer between prints, cover and allow to settle for ~5 min, then heat to 125 °C for 10 min before returning to the printer to print a subsequent layer.
4. Once the final print is made run a full sinter program. Heat the electrodes to 150 °C at 12.5°/min, hold 10 min, then to 325 °C at 11.7 °/min, hold 5 min, then to 375 °C at 10 °/min, hold 5 min, then to 450 °C at 10.7 °/min, hold 30 min and finally to 500 °C at 10 °/min, hold 15 min. Slowly cool to RT after this.
5. Cut the master plate into individual electrodes ensuring there is sufficient room around the printed film for the gasket to be applied after. Remove any glass shards using compressed air.
6. Immerse electrodes in a 20 mM $TiCl_4$ solution (aq.), cover loosely and place container in a preheated oven (70 °C for 30 min). Subsquently, wash the electrodes thoroughly and sinter once more at 500 °C for 30 min.
7. Once cooled to below 100 °C, immerse the electrodes in a 0.5 mM dye solution. In this case use, D149 in acetonitrile:tertbutanol (1:1).
8. After dyeing O/N remove the electrodes and rinse vigorously in acetonitrile for ~30 sec then allow to sit for a further 30 sec. Withdraw electrodes from the rinsing bath and dry with compressed air.

1.2. Counter Electrode Preparation

1. Cut another sheet of 2.3 mm F:SnO_2 glass into 18.3 mm × 27.5 mm pieces.
2. Immerse counter electrode in water and drill a small hole in the corner (φ = 1 mm, 2.5 mm from each corner) to use as a filling port, using a diamond tipped dental burr mounted in a small bench drill.
3. Clean counter electrode as per section 1.1.1
4. Dry counter electrode and place on a tile with conductive side up. Apply one drop of platinic acid solution (H_2PtCl_6, 10 mM in ethanol) and spread with the end of a pipette. Place tile onto preheated (400 °C) hotplate for 15 min. After this, remove glass and tile and allow to cool on a bench.

1.3. Reflector

1. Cut a piece of nonconductive 2 mm glass to 18.3 mm × 27.5 mm and drill two holes in adjacent corners along the long edge, using the same technique as for the counter electrode (section 1.2.2).
2. Clean glass, once using the same protocol as above (1.1.1)
3. Tape the clean, dry glass to the bench on three sides, using low residue tape. Apply a drop of Al_2O_3 paste (2.0 g of 0.3 µm Al_2O_3 particles, 2 ml colloidal Al_2O_3 + 1 ml ethanol) and draw down with a glass rod.
4. Allow film to dry, remove tape and sinter glass at 500 °C for 30 min.

1.4. Device Assembly

1. Cut two batches of hot melt adhesive gaskets.
   NOTE: The first, for the DSC, is 25 µm thick and has internal dimensions of 17 mm × 8 mm and external dimensions of 21 mm × 12 mm. The sec, for the upconversion chamber, uses 60 µm gasket material doubled over to give 120 µm thickness. When folded, this gasket has internal dimensions of 17 mm × 21 mm and external dimensions of 21 mm × 25 mm.
2. Place the first gasket in the corner of the counter electrode, ensuring the filling port is accessible. Place the working electrode over this, such that the printed area is entirely inside the gasket, and obtain a good seal.
3. Move this assembly to a hotplate (120 °C) and apply pressure until gasket softens and melts, which can be observed visually as the gasket wets the glass surfaces. Remove assembly and allow to cool.
4. Place second gasket on reflector, once again ensuring filling ports are not covered. Place DSC on top such that the printed area is directly in front of the printed alumina reflector. Once again heat device while applying pressure, until gasket softens and adheres, as in section 1.4.3. This assembly is shown in **Figure 1**.

1.5. Filling Cavities

1. Prepare an electrolyte solution of 0.1 M LiI, 0.6 M 1,2-dimethyl-3-propylimidazolium iodide and 0.05 M iodine in methoxypropionitrile.
2. Place the device in a small plastic container with vacuum tube attached, with the counter electrode facing upwards.
3. Put a drop of the electrolyte solution over the hole and a piece of glass on top. Apply vacuum for a few sec to extract air from the DSC cavity, before releasing, which will draw electrolyte into the cavity.
4. Prepare the seals by laminating hot melt gasket material onto aluminum foil. Leave these on a hotplate, gasket material side up. Clean the back of the counter electrode thoroughly, then seal by pressing device against the gasket material for ~5 sec.
5. Prepare TTA-UC solution by dissolving 0.6 mM of Pd dye (tetrakis(3,5-di-tert-butylphenyl)-6'-amino-7'-nitro-tetrakisquinoxalino[2,3-b'7,8-b"12,13-b"'17,18-b""-porphyrinato) palladium(II)) and 22 mM of rubrene in benzene. Deaerate this solution thoroughly using three liquid nitrogen freeze-pump-thaw cycles.
6. Inside a glovebox, introduce the TTA-UC solution into the back cavity, allowing capillary forces to draw it through. Once full, once again clean the surface thoroughly and seal using another piece of aluminum backed gasket material.

2. Measurement

2.1. Electrical Contacts

1. Apply solder to exposed F:SnO_2 of working and counter electrodes using sonic soldering iron and appropriate solder.
2. Attach wires to anode and cathode using normal solder.
3. Apply UV curable epoxy to open edges.
   NOTE: This is done to serve as a secondary encapsulation of the device against oxygen ingress and solvent evaporation, as well as increasing the robustness of the device, particularly the wire attachment.
4. Attach the anode and cathode wire to an open-ended BNC cable through a terminal block.

2.2. IPCE Measurement Setup

1. Using the setup shown schematically in **Figure 2**, mount the integrated device onto a cell holder.
2. Illuminate a section of the integrated device (~2 mm × 1 mm) with a 670 nm continuous wave laser beam (the 'pump beam') via a mirror on an adjustable mount.
3. Illuminate the integrated TTA-UC DSC with incoherent quasi-monochromatic light (the 'probe beam') generated using an Xe lamp, passed first through a 405 nm longpass filter, then a chopper wheel operating at 29 Hz, a monochromator, an angled glass slide (used here as a ~4% beam splitter) and a parabolic mirror. Generate a background triplet population in the TTA-UC layer by exciting the UC layer with the pump beam, which is incident at such an angle that it does not illuminate the probed DSC active layer but the UC layer only.
4. Align the pump and probe beam on the TTA-UC layer using the adjustable mirror mount. Measure the short circuit current generated by the probe as it is scanned across the visible spectrum in 5 nm increments using a dynamic signal acquisition device, current amplifier and in-house control software.
5. Simultaneously record the power variation of the probe beam reflected from the glass slide with a power meter and a photodiode with analog output fed to the signal acquisition device. Correct the J_{SC} from the device by the probe variation in the software.
6. Displace the pump beam slightly using the adjustable mirror mount, such that it hits the active layer of the device adjacent to the probe beam. Repeat the measurement with the pump and probe beam misaligned.
7. Record six sets of measurements with alignment and misalignment at the same positions for better signal to noise ratio.
8. Reduce the pump beam intensity by placing on the pump beam different neutral density filters with known transmissions at 670 nm, and repeat steps 2.2.4 to 2.2.7 for a range of intensities.
9. Measure the integrated device J_{SC} without the pump beam source active.
10. Measure the probe power incident on the DSC in terms of current generated by the photodiode by placing the photodiode at the sample position.
11. Measure the transmission of the studied device with the UC chamber removed using a UV Visible Spectrophotometer to obtain the transmission spectrum, T_{DSC}.
    NOTE: This may be alternately done in between steps 1.4 and 1.5.

2.3. Pump Source Characterization

1. Measure the pump beam power at the DSC position for each filtering condition used, using the photodiode and power meter (as described in section 2.2.10).

2. Take a photograph of the pump beam projecting onto a piece of grid paper at a position equivalent to where the TTA layer was during the experiment. Heavily attenuate the beam if necessary to prevent saturation of the camera detector. Use this image and image analysis software to determine the pump spot size.

3. Data processing

3.1. Interpolate All Data to 1 nm Increments.

3.2. IPCE Determination

1. Calculate the photon flux (φ) reaching the integrated device from the probe power measured as current generated by the photodiode (*I*) and electric charge (*q*):
2. Calculate the cell incident photon to converted electron efficiency ($IPCE_0$) of the device from the J_{SC} measurement without pump illumination and the probe flux.
3. Take the ratios between measurements with pump and probe aligned and misaligned to obtain the relative enhancements from activating the up-convertor.
4. Solar concentration factor determination
5. Convert the extinction coefficient of the sensitizer into absorption cross section, σ.
6. Obtain the excitation rate of the sensitizer under the standard AM1.5G solar spectrum, ($k_φ$) by taking the products of photon flux density from the solar spectrum, transmittance of the DSC and the sensitizer (σ) at each wavelength and then summing the products across the sensitizer Q-band absorption, typically 600 nm to 750 nm.
7. Calculate, from the powers and spot size of the pump source, the photon flux densities of the pump with different neutral density filters. Then take the products of the flux densities, transmittance of the DSC and the sensitizer at 670 nm to obtain the pump excitation rates.
8. Calculate the solar concentration factor (Θ) from the ratio of pump excitation rate to the excitation rate under AM1.5G conditions.

3.3. Model Fitting and Figures of Merit Determination

1. Fit a model of the relative enhancement = 1 + constant × (T_{DSC}/$IPCE_0$) × [($σ_{pump}$× $σ_{probe}$) / ($σ_{pump}$ + $σ_{probe}$)], onto the experimental enhancement results, where $σ_{pump}$ and$_{σprobe}$ are cross-sections with respect to the pump and probe wavelengths; $σ_{pump}$ is fixed for each pump intensity and $σ_{probe}$ varies with wavelength.
2. Estimate the enhancement in J_{SC} obtained from the upconversion effect ($ΔJ_{SC}$) from the differences between $IPCE_{UC}$ and $IPCE_0$ and the solar flux density.
3. Calculate the FoM by normalizing $ΔJ_{SC}$ by the square of solar concentration factor, since TTA-UC has a quadratic dependence on power input at low excitation intensity.

Representative Results

Figures 3A - **D** display enhancement responses measured under different measurement conditions, with the effects discussed in more detail below. From the raw current density enhancements it should be clear that the results in **Figure 4A** and **4B** are attributable to upconversion, with the peak current enhancement and IPCE enhancement matching well with the absorption spectrum of the sensitizer, attenuated by transmission through the active layer of the DSC.

In order to avoid measurement artifacts introduced by laser biasing the pump beam has been adjusted to arrive at the UC layer at a greater angle to the probe beam, shown schematically in **Figure 2**. **Figure 4A** shows enhancement without significant biasing effect, whereas both **Figures 4C** and **4D** are affected by this problem. The consequence of correct alignment on measurements is shown in **Figure 4A** where the difference in J_{SC} reflects the absorption property of the sensitizer which has an absorption peak at 675 nm. Apart from the absorption region of the sensitizer and the transparent region of the device, the difference in J_{SC} is embedded in noise.

A significant relative IPCE enhancement of the integrated device in the red end of visible spectrum can be observed in **Figure 4C**. However, the insert of **Figure 4C** which shows the difference between aligned and misaligned J_{SC} measurements, does not reflect the spectral property of the sensitizer. The alignment of pump and probe seem to enhance the cell performance across the entire visible spectrum and suggests that the enhancement comes from trap-filling which enhances the overall performance of the device, due to laser biasing[30].

In order to verify the suspicion, the integrated device was replaced by an analogous device except that the UC chamber was left empty (**Figure 4D**). Under the identical experimental condition, enhancement has been found across the visible spectrum. It confirms the previous enhancement effect comes from laser-biasing instead of TTA-UC. In the case of the device without TTA-UC solution, since the majority of the laser is scattered back to the device, the biasing effect is even more significant.

Figure 5 expands upon the results shown in **Figures 4A** and **4B**. In this case, the light intensity of the pump beam was adjusted from 6 to 27 Θ. $ΔJ_{SC}$ is seen to scale with the square of light intensity, as per expectation (power law fit 2.02). As such, the FoM is seen to be light intensity independent, suggesting that the TTA-UC system is limited by bimolecular processes.

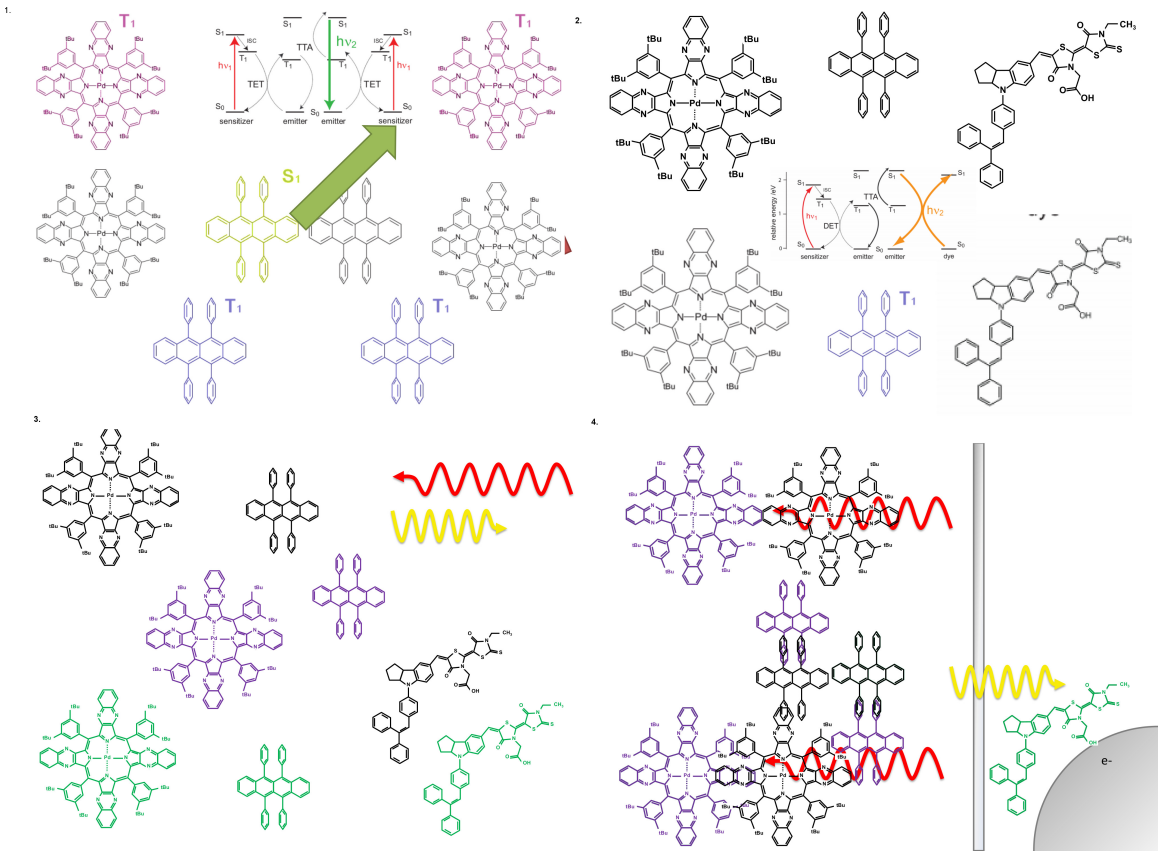

Animation 1: Schematic operation of triplet-triplet annihilation photon up-conversion with PQ4PdNA sensitizer and rubrene emitter, resulting in illumination of D149 dye and subsequent electron injection into TiO_2. Please click here to view a larger version of this figure.

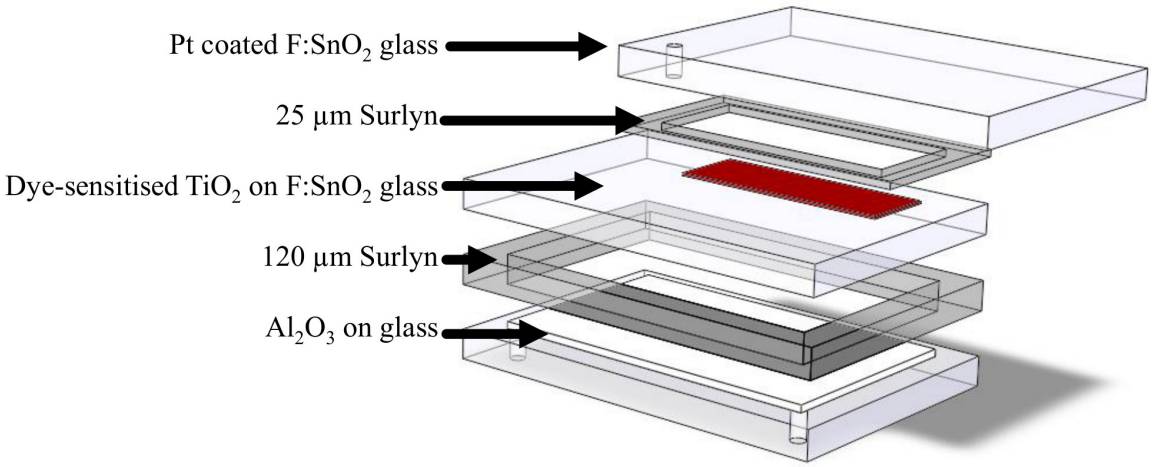

Figure 1. Device configuration, prior to introduction of liquid components. Layers are placed together and sealed by application of heat to soften the gasket layers. Please click here to view a larger version of this figure.

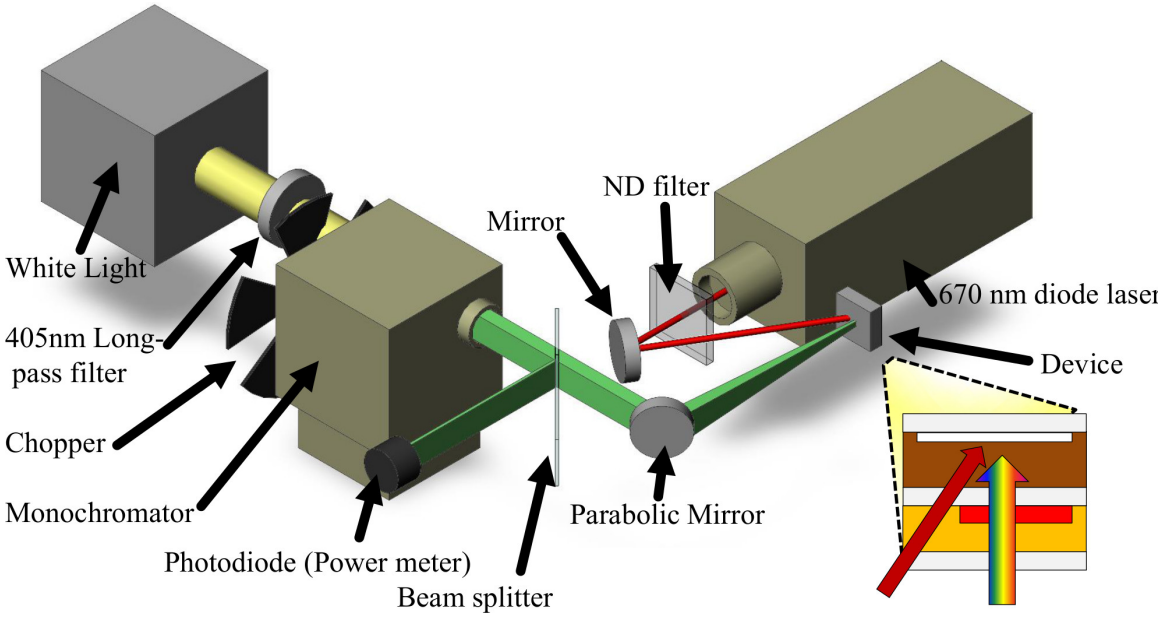

Figure 2. Setup for the enhancement measurement. The integrated device is irradiated by modulated incoherent monochromatic light from a white light source (laser-driven lamp) passed through a monochromator, and achromatically focused onto the sample by an off-axis parabolic mirror. The probe light is split with a glass filter (beam slitter) and the reflected probe light is detected by a photodiode attached to a power meter. The TTA-UC layer of the integrated device is continuously excited by a 670 nm continuous wave laser (pump) to generate background triplets to allow the TTA-UC enhancement effect to be probed with the weak monochromatic beam. The output current from the device is fed through a current amplifier and measured by lock-in amplification. Please click here to view a larger version of this figure.

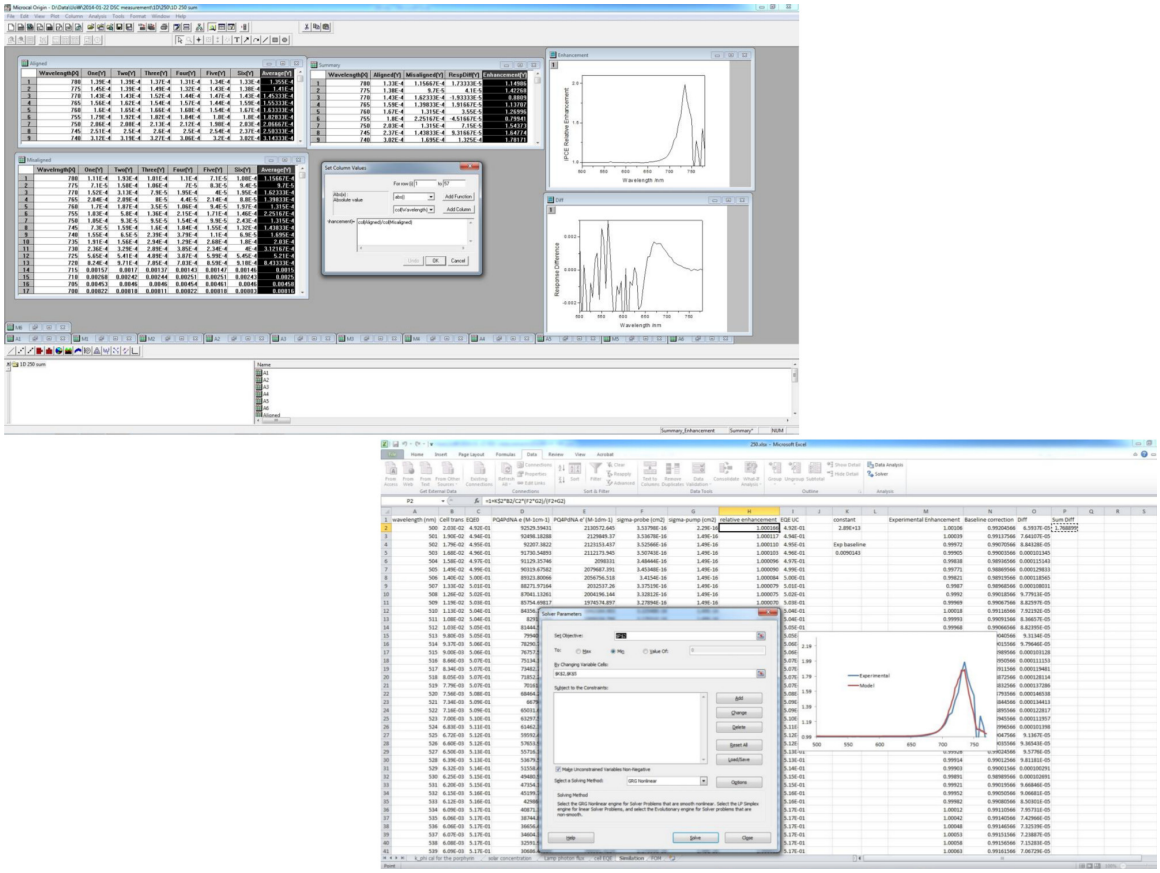

Figure 3. Representative data showing **(A)** the relative IPCE enhancement (col(Aligned)/col(Misaligned) and response difference (col(Aligned)-col(Misaligned) averaged from six aligned and six misaligned measurements. The response difference confirms the spectral shape of IPCE enhancement is from sub-bandgap light harvested by the sensitizer of the up-convertor, as the enhancement spectral shape matches to the Q-band absorption of the sensitizer and **(B)** the relative enhancement model fitted (described previously[31]) onto an experimental IPCE enhancement curve by least-squares fitting. The model includes cell transmittance, the original cell IPCE (no pump) and the sensitizer absorption cross section corresponding to probe and pump source. The modeled enhancement curve is then used for calculating additional short-circuit current generated from TTA-UC and thus FoM. Please click here to view a larger version of this figure.

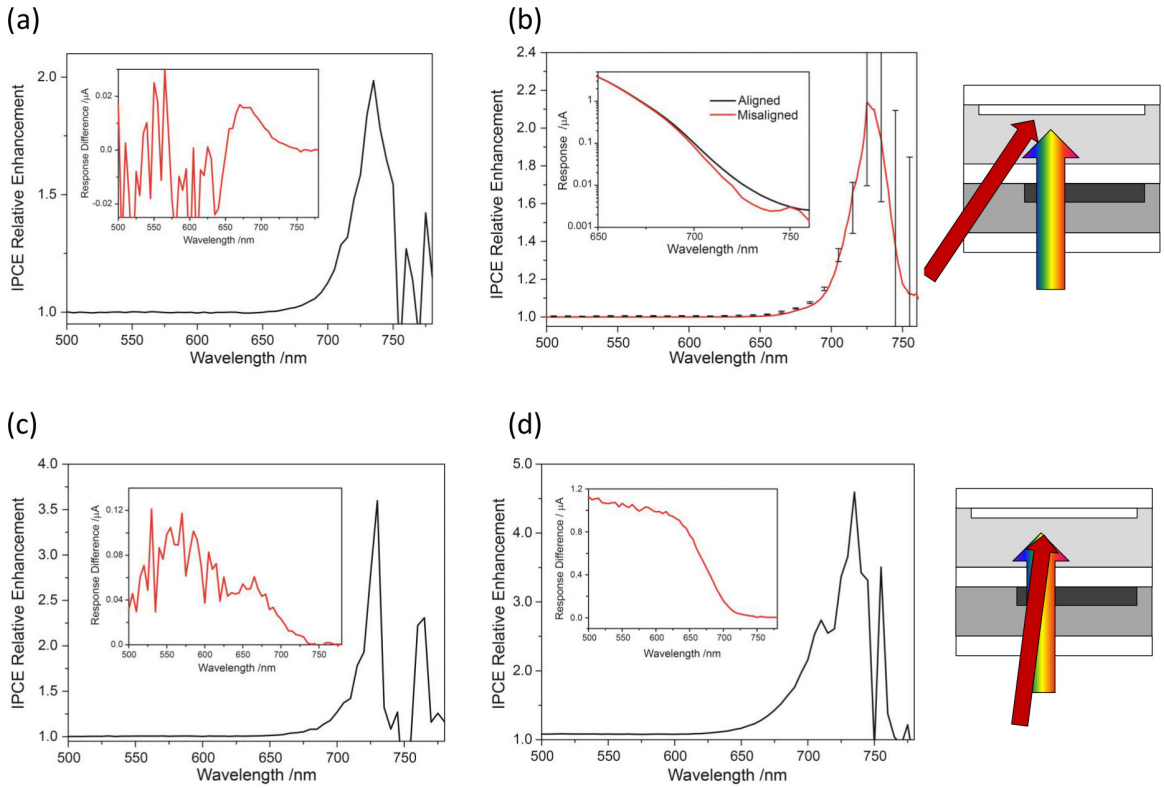

Figure 4. IPCE enhancement (under 27 ʘ) traces for **(A)** an integrated device with correct misalignment measurement (inset showing the gain in raw response), **(B)** modeled relative IPCE enhancement trace for data in **(A)** with inset showing the raw current response curves of the device with pump and probe beam aligned and misaligned **(C)** the same device as in **(A)** excepting that the pump and probe being aligned at the same site on the active electrode, resulting in a measurement artifact, described in the text **(D)** an identical device with an empty UC chamber, measured as per **(C)**, further highlighting this measurement problem, with inset showing the gain in raw response. Please click here to view a larger version of this figure.

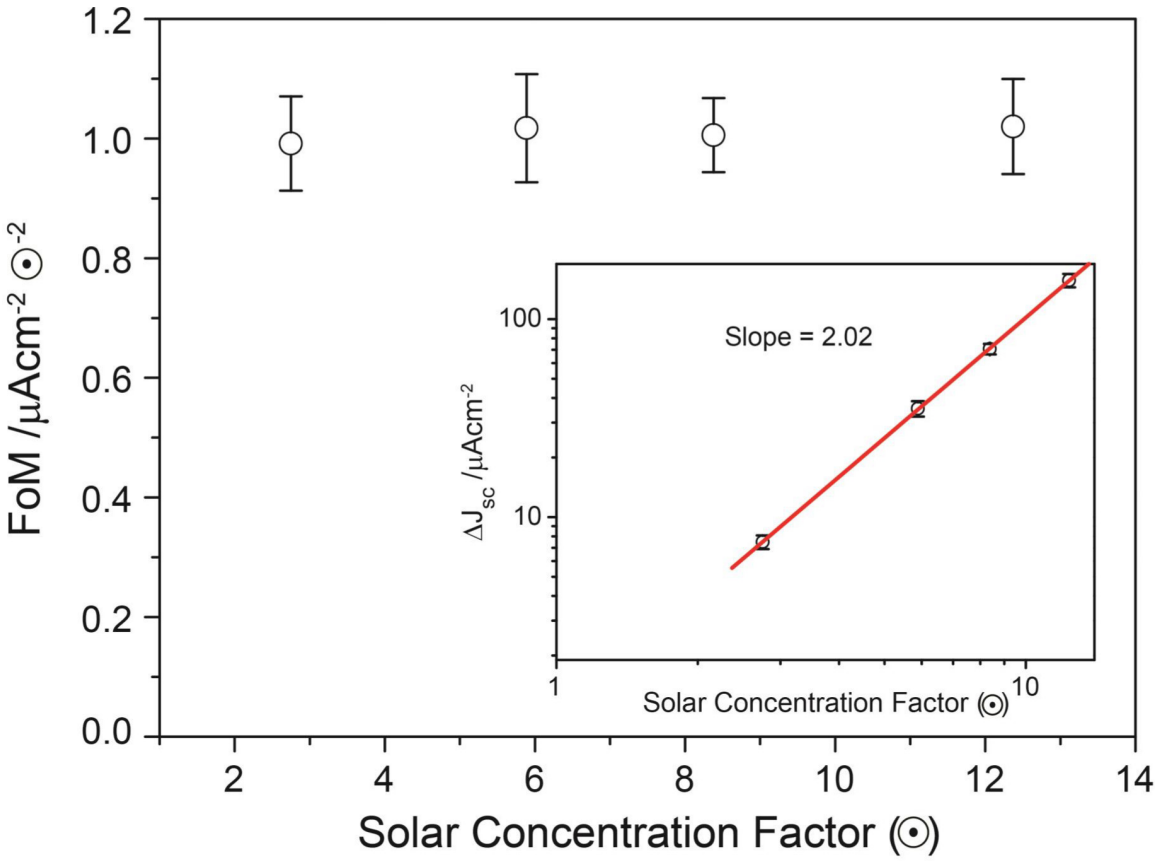

Figure 5. FoM dependence of the integrated device on solar concentration factor. Inset shows the dependence of calculated current gain (ΔJ_{SC}) from TTA-UC with both axes on a logarithmic scale.

Discussion

This protocol provides a means to achieve photon up-conversion enhanced DSC and detail on how to correctly measure such a device. The FoM allows for the simple calculation of anticipated ΔJ_{SC} improvements to be expected at different light intensities, including at 1 sun. The values shown here are invariant with light intensity (inset of **Figure 4**), as per expectation when the system is below its saturation threshold[33]. With the FoM, we can standardize the enhancement effect of TTA-UC or other non linear UC processes to allow easy comparison.

Although the FoM values obtained in this study are the highest among the reported FoMs for DSCs, they are still far from commercial interest (~1 $mA{\cdot}cm^{-2}\odot^{-2}$). In addition to this, enhancements of this scale can be problematic to measure. In this report (specifically in **Figures 3C** and **3D**) the perils of incorrect measurement technique are shown, where the pump beam causes a (somewhat) unexpected problem. This issue may be unique to DSCs, however if there is any uncertainty it is crucial that control experiments (such as shown in **Figure 3D**) are undertaken and conditions modified accordingly.

There are a few limiting factors that restrict the performance of TTA-UC. First of all is the triplet decay rate of the emitter, rubrene (~8,000 sec^{-1}[34]), which is much faster than the excitation rate of the sensitizer under 1 ʘ illumination (6.8 sec^{-1}), while the TTA rate of rubrene triplets is only ~1 × 10^8 $M^{-1}sec^{-1}$, three orders of magnitude below the diffusion limit of rubrene in common organic solvents[35]. The consequence of this is the majority of triplet rubrene decays to the ground state before performing TTA.

In order to reduce the amount of rubrene triplets undergoing unimolecular decay before TTA one can attempt to increase the triplet concentration, by increasing the sensitizer concentration. Unfortunately, porphyrins in solution tend to aggregate at high concentrations, and sensitizer-sensitizer TTA may take place. A potential solution overcome these issues is to attach sensitizers onto inorganic nanoparticle surfaces[36]. As such, high concentrations of (relatively) immobilized sensitizer can be accommodated with reduced self-quenching, and may increase the local concentration of triplets available for efficient TTA.

The sensitizer used in this study is not ideal for the coupled DSC, as the Q-band absorption of the porphyrin overlaps with the DSC's absorption onset (600 - 700 nm). Thus there are losses in transmitted light available for TTA-UC, the efficiency of which depends on triplet concentration and thus photon flux. We expect to measure a more significant enhancement with a sensitizer that absorbs deeper into the near infrared with similar intersystem crossing efficiency to the one used in this study. The FoM offers a convenient metric of comparison, if and when such a system is characterized.

The dye used here, D149, is among the best performing organic dyes available for DSC, however others, such as N719 or "black dye" have further red-shifted absorption onsets[3]. In order for TTA-UC to enhance these devices, appropriate porphyrins with Q-band absorptions at

wavelengths greater than 900 nm need to created. On the other hand, the highest reported DSC efficiency to date has an absorption onset of ~730 nm[37], only marginally beyond the onset for the dye used here.

Disclosures

There is nothing to disclose.

Acknowledgements

A.N. acknowledges contributions from the Australian Renewable Energy Agency (ARENA) and the Australian National Fabrication Facility (ANFF). This research project is funded by the Australian Solar Institute (6-F020 and A-023), with contributions from The New South Wales Government and the University of Sydney. Aspects of this research were supported under Australian Research Council's Discovery Projects funding scheme (DP110103300). Equipment was purchased with support from the Australian Research Council (LE0668257).

References

1. Regan, B., & Grätzel, M. A low-cost, high-efficiency solar-cell based on dye-sensitized colloidal TiO_2 films. *Nature.* **353,** 737-740, 10.1038/353737a0 (1991).
2. Grätzel, M. Photoelectrochemical cells. *Nature.* **414** (6861), 338-344, 10.1038/35104607 (2001).
3. Hagfeldt, A., Boschloo, G., Sun, L., Kloo, L., & Pettersson, H. Dye-Sensitized Solar Cells. *Chem. Rev.* **110** (11), 6595-6663, 10.1021/cr900356p (2010).
4. Tayebjee, M.J.Y., Hirst, L. C., Ekins-Daukes, N. J., & Schmidt, T. W. The efficiency limit of solar cells with molecular absorbers: A master equation approach. *J. Appl. Phys.* **108**, 124506, 10.1063/1.3517826 (2010).
5. Daeneke, T., Gräf, K., Watkins, S. E., Thelakkat, M., & Bach, U.*Infrared Sensitizers in Titania-Based Dye-Sensitized Solar Cells using a Dimethylferrocene Electrolyte. ChemSusChem.* **6**, 2056-2060 (2013).
6. Tian, H. N., Yang, X., Chen, R., Hagfelt, A., & Sun, L. A metal-free 'black dye" for panchromatic dye-sensitized solar cells. *Energ. Environ. Sci.* **2** (6), 674-677, 10.1039/b901238a (2009).
7. Daeneke, T.*, et al.* Dye Regeneration Kinetics in Dye-Sensitized Solar Cells. *J. Am. Chem. Soc.* **134** (41), 16925-16928, 10.1021/ja3054578 (2012).
8. Green, M.A. *Third Generation Photovoltaics: Advanced Solar Energy Conversion.* Springer Series in Photonics, New York, NY (2003).
9. He, J.J.*,* Lindström, H., Hagfeldt, A., & Lindquist, S. E. Dye-sensitized nanostructured p-type nickel oxide film as a photocathode for a solar cell. *J. Phys. Chem. B.* **103** (42), 8940-8943 (1999).
10. Nattestad, A.*, et al.* Highly efficient photocathodes for dye-sensitized tandem solar cells. *Nat. Mater.* **9** (1), 31-35, 10.1038/nmat2588 (2010).
11. Nattestad, A.*, et al.* Dye-Sensitized Solar Cell with Integrated Triplet-Triplet Annihilation Upconversion System. *J. Phys. Chem. Lett.* **4** (12), 2073-2078, 10.1021/jz401050u (2013).
12. Liu, M., Lu, Y., Xie, Z. B., & Chow G. M. Enhancing Near-Infrared Solar Cell Response Using Upconverting Transparent Ceramics. *Sol. Energ. Mat. Sol. C.* **95**, 800-803, 10.1016/j.solmat.2010.09.018 (2011).
13. Shan G. B., & Demopolous, G. P. Near-Infrared Sunlight Harvesting in Dye-Sensitized Solar Cells Via the Insertion of an Upconverter-TiO_2 Nanocomposite Layer. *Adv. Mater.* **22***,* 4374-4377, 10.1002/adma.201001816 (2010).
14. Yuan, C., *et al.* Use of Colloidal Upconversion Nanocrystals for Energy Relay Solar Cell Light Harvesting in the Near-Infrared Region. *J. Mater. Chem.* **22**, 16709-16713, 10.1039/c2jm16127c (2012).
15. Cheng, Y.Y.*, et al.* In Next Generation (Nano) Photonic and Cell Technologies for Solar Energy Conversion. *Molecular Approaches to Third Generation Photovoltaics: Photochemical Up-conversion*. 7772-7 (2010).
16. Parker, C.A., & Hatchard, C. G. Delayed Fluorescence from solutions of Anthracene and Phenanthracene. *P. R. Soc. London.* **269**, 574-584, 10.1098/rspa.1962.0197 (1962).
17. Zhao, J., Ji, S., & Guo, H. Triplet-Triplet Annihilation Based Upconversion: From Triplet Sensitizers and Triplet Acceptors to Upconversion Quantum Yields. *RSC Adv.* **1**, 937-950, 10.1039/c1ra00469g (2011).
18. Singh-Rachford, T. N., & Castellano, F. N. Photon Upconversion Based on Sensitized Triplet-Triplet Annihilation. *Coordin. Chem. Rev.* **254**, 2560-2573, 10.1016/j.ccr.2010.01.003 (2010).
19. Baluschev, S., *et al*. Up-Conversion Fluorescence: Noncoherent Excitation by Sunlight. *Phys. Rev. Lett.* **97**, 143903, 10.1103/PhysRevLett.97.143903 (2006).
20. Ceroni, P. Energy Up-Conversion by Low-Power Excitation: New Applications of an Old Concept. *Chem. Eur. J.* **17**, 9560-9564, 10.1002/chem.201101102 (2011).
21. Penconi, M.*,* Ortica, F., Elisei, F., & Gentili, P. G. New Molecular Pairs for Low Power Non-Coherent Triplet-Triplet Annihilation Based Upconversion: Dependence on the Triplet Energies of Sensitizer and Emitter. *J. Lumin.* **135**, 265-270, 10.1016/j.jlumin.2012.09.033 (2013).
22. Liu, Q., Yang, T., Feng, F., & Li F.*Blue-Emissive Upconversion Nanoparticles for Low-Power-Excited Bioimaging in Vivo. J. Am. Chem. Soc.* **134**, 5390-5397, 10.1021/ja3003638 (2012).
23. Simon Y.C., & Weder, C. Low-Power Photon Upconversion through Triplet-Triplet Annihilation in Polymers. *J. Mater. Chem.* **22**, 20817-20830, 10.1039/c2jm33654e (2012).
24. Jankus, V., *et al.* Energy Conversion via Triplet Fusion in Super Yellow PPV Films Doped with Palladium Tetraphenyltetrabenzoporphyrin: a Comprehensive Investigation of Exciton Dynamics, *Adv. Funct. Mater.* **23**, 384-393, 10.1002/adfm.201201284 (2013).
25. Cheng, Y. Y., *et al.* Entropically Driven Photochemical Upconversion. *J. Phys. Chem. A.* **115**, 1047-1053, 10.1021/jp108839g (2011).
26. Cheng, Y. Y.*, et al.* Kinetic Analysis of Photochemical Upconversion by Triplet-Triplet Annihilation: Beyond Any Spin Statistical Limit. *J. Phys. Chem. Lett.* **1** (12), 1795-1799, 10.1021/jz100566u (2010).
27. Baluschev, B., *et al.* Upconversion with ultrabroad excitation band: Simultaneous use of two sensitizers. *Appl. Phys. Lett.* **90**, 181103, 10.1063/1.2734475 (2007).

28. Borjesson, K., *et al.* Photon upconversion facilitated molecular solar energy storage. *J. Mater. Chem. A.* **1**, 8521-8524, 10.1039/c3ta12002c (2013).
29. Cheng, Y.Y., *et al.* Improving the light-harvesting of amorphous silicon solar cells with photochemical upconversion. *Energ. Environ. Sci.* **5** (5), 6953-6959, 10.1039/c2ee21136j (2012).
30. Dominici, L. Dye-Sensitized Solar Cells: Basic Photon Management Strategies, *Solar Cells – Dye-Sensitized Devices.* (ed. Kosyachenko, L.A.) *InTech*, 291 (2011).
31. Schulze, T. F., *et al.* Photochemical Upconversion Enhanced Solar Cells: Effect of a Back Reflector. *Aust. J. Chem.* **65** (5), 480-485, 10.1071/CH12117 (2012).
32. Schulze, T. F., *et al.* Efficiency Enhancement of Organic and Thin-Film Silicon Solar Cells with Photochemical Upconversion. *J. Phys. Chem. C.* **116** (43). 22794-22801, 10.1021/jp309636m (2012).
33. Haefele, A., Blumhoff, B., Khnayzer, R. S., & Castellano, F.*Getting to the (Square) Root of the Problem: How to Make Noncoherent Pumped Upconversion Linear. J. Phys. Chem. Lett.* **3**, 299-303, 10.1021/jz300012u (2012).
34. Lewitzka F., & Löhmannsröben, H. G. Investigation of Triplet Teracene and Triplet Rubrene in Solution. *Z. Phys. Chem.* **150**, 69-86 (1986).
35. Ventura, B., Esposti, A. D., Koszarna, B., Gryko, D. T. and Flamigni, L. Photophysical characterization of free-base corroles, promising chromophores for light energy conversion and singlet oxygen generation. *New J. Chem.* **29**, 1559-1566, 10.1039/b507979a (2005).
36. MacQueen, R.W., *et al.* Nanostructured upconverters for improved solar cell performance. *Proceedings SPIE.* **8824**, 882408-882408-9, 10.1117/12.2026907 (2013).
37. Yella, A., *et al.* Porpyrin-sensitized Solar Cells with Cobalt (II/III)-based redox electrolyte exceed 12 percent efficiency. *Science.* **334**, 629-634, 10.1126/science.1209688 (2011).

